Geochemical, mineralogical and geostatistical modelling of an IOCG tailings deposit (El Buitre, Chile): implications for environmental safety and economic potential

Erika González-Díaz[a,b], Sebastián García[b,c], Fabián Soto[b,c,d], Felipe Navarro[b,d], Brian Townley[a,b], Manuel A. Caraballo[b,c,e,f*]

[a] *Geology Department, University of Chile, Plaza Ercilla 803, Santiago, Chile*

[b] *Advanced Mining Technology Center, University of Chile, Avda. Tupper 2007, 8370451 Santiago, Chile*

[c] *Mining Engineering Department, University of Chile, Avda. Tupper 2069, Santiago, Chile.*

[d] *Advanced Laboratory for Geostatistical Supercomputing (ALGES), Universidad de Chile, Avenida Tupper 2069, Santiago, Chile*

[e] *Department of Water, Mining and Environment, Scientific and Technological Center of Huelva, University of Huelva, 21004 Huelva, Spain*

[f] *Department of Mining, Mechanic, Energetic and Construction Engineering, Higher Technical School of Engineering, University of Huelva, Avda. de las Fuerzas Armadas, S/N, 21071 Huelva, Spain*

Corresponding authors:

Manuel A. Caraballo macaraballomonge@gmail.com;

Erika González-Díaz, egonxalez@ing.uchile.cl;

Phones: (+56) 2 29784479/ (+56) 988856604

Abstract:

In the mining industry deposits of tailings represent large volumes of the mining wastes, reflecting the mineralogy and chemistry of the ore deposit type of origin. In this paper, we report the results of a mineralogical and geochemical characterization study and geostatistical modelling of an Iron Oxide Copper Gold deposit with neutral pH, in an arid climate. Twenty-eight boreholes allowed recovery of 755 samples for analysis. Modelling by means of co-kriging spatial interpolation allowed determination of the distribution of concentrations for elements of interest in the deposit. Low water flow and near neutral-pH paste restrict the mobility of the chemical elements, limiting the development of an oxidation front and inhibiting the appearance of a secondary mineral enrichment zone and the precipitation of secondary efflorescent salts on the tailings surface. Our observations determine that the composition of the gangue material, and to a lesser extent the effect of the tailings gravitational deposition and the geometry of the deposit, control the geochemical and mineralogical associations and distributions present in this deposit of tailings. The observed low mobility along the tailings profile of some potential pollutants (e.g., As, Mn, Cr and Ni) allows to anticipate a low groundwater pollution risk as long as the current environmental conditions remain. Additionally, the depositional history of the tailings had a great influence on the vertical and horizontal distribution of pyrite. However, the grades of elements economic interest such as Fe, Cu and Co are uniformly distributed, which would facilitate the application of tailings reprocessing technologies. In addition, it would allow maximizing the number of necessary boreholes for its economic evaluation.

Keywords: Fe oxide Cu–Au deposits, Tailings, Conceptual model, Neutral pH, Arid climate.

1. Introduction

The deposits of tailings could contain multiple elements considered to be of strategic interest, which were not extracted in the past, either because they were not considered to be of economic value, or due to the lack of appropriate technologies for their economic recovery (Lottermoser, 2010; Pan et al., 2014). In addition, a recent study by Franks et al., (2021) have estimated the presence of more than 8,100 tailings deposits globally and the generation of 10 billion m^3 of fresh tailings every year. As a result, deposits of tailings have become a focus of interest as possible alternative sources of raw materials to partially mitigate the shortages on many critical raw elements imposed by the always growing demand of technological applications and green energies (Parviainen et al., 2020). The economic potential of these types of waste has been demonstrated in various tailings worldwide (Araya et al., 2021; Araya et al., 2020; Ceniceros-Gómez et al., 2018; Dino et al., 2018; Falagán et al., 2017; Moran-Palacios et al., 2019; Pan et al., 2014; Parbhakar-Fox et al., 2018; Parviainen et al., 2020). Complementary, there are also numerous studies dealing with the environmental characterization of mine tailings (Buch et al., 2021; Cleaver et al., 2021; Lam et al., 2020, 2021) and proposing different reutilization alternatives, such as transforming them into ceramics and construction materials (Kang et al., 2021; Krishna et al., 2021; Zhang et al., 2021).

The deposits of tailings exposed to the environment are susceptible to weathering. In consideration of supergene, processes that affect these deposits, and based on present knowledge the following aspects should be considered:

1) The presence of minerals such as calcite, dolomite and, to a lesser extent, some aluminosilicates, can effectively neutralize the acidity generated and maintain circum-neutral pH conditions (Blowes et al., 1998; Lindsay et al., 2009a);

2) The mobility of liberated elements by oxidation, leaching and neutralization reactions depends on the climatic conditions, the geometry of the deposit and multiple biogeochemical processes, including precipitation/dissolution, or redox;

3) Stratifications within the deposits of tailings are determined by: *i*) the mineralogy of the source reservoir, *ii*) the grain size distribution and *iii*) ore mineral liberation resulting from the mineral processing stage, and *iv*) the gravitational segregation processes during the settlement of the tailings (Dold and Fontboté, 2001, 2002; Kovács et al., 2006; Heikkinen and Räisänen, 2008; Marescotti et al., 2010; Pan et al., 2014; Wang et al., 2017).

Several characterization studies have been carried out on tailings from sulfide-rich mineral deposits, such as copper porphyry, skarn, volcanogenic massive sulfide, among others (Dold and Fontboté, 2001; Lindsay et al., 2009a; Lindsay et al., 2009b; Hällström et al., 2018). Dold and Fontboté (2001) determined that the deposit of tailings generated from copper porphyry deposits have a low neutralization potential associated with the low carbonate content and the relatively high content of minerals derived from supergene enrichment. These characteristics, together with favorable climatic conditions and long exposure time of the tailings typically lead to the development of acid mine drainage (Smuda et al., 2014). Skarn-type deposit materials are considered high in carbonates, sulfides, and fluorite. As a result, their deposit of tailings frequently exhibit high mobility of metals due to the pH decrease induced by iron-sulfides oxidative dissolution (Blowes et al., 2003) and complexation with F ions keeping metals mobile (Petrunic and Al, 2005). On the other hand, tailings deposits with low-sulfur and high-iron (Henne et al., 2020), like the deposits generated after the mineral processing of Iron Oxides Copper Gold (IOCG) or Iron Oxide-Apatite (IOA) type deposits have been barely studied (Dold and Fontboté, 2002; Henne et al., 2019; Medina et al., 2019) and their weathering and evolution in arid and semi-arid climates is poorly understood.

IOCG-type ore deposits are globally distributed, grouping different styles of mineralization. Only eleven IOCG provinces “sensu stricto” have been recognized worldwide, including the Central Andean Coastal Belt, spanning from Southern Peru to Northern Chile (Sillitoe, 2003). In recent decades they have been considered profitable exploration targets due to the economic recovery of copper, gold and other by-products such as uranium (Barton, 2014). These deposits may also contain high concentrations of rare earth elements (REEs), silver, molybdenum, nickel, cobalt, barium, fluorine, and phosphorus (Barton, 2014). Most of these elements are on the European Commission’s list of critical raw materials due to their economic importance and supply risk (European Commission, 2017).

In Chile there are more than 757 deposits of tailings, of which 173 are abandoned and 467 are inactive. More than 80 % are located in the north of the country where the climatic conditions are arid and semi-arid and where the main IOCG deposits are located (e.g., Manto Verde, Punta del Cobre, Cerro Negro, El Espino and Candelaria) (Sernageomin, 2020a). Due to the difficulties and costs of drilling these deposits and the low economic potential they are thought to represent, most tailings studies in Chile (and around the world) are usually limited to near surface samples, depths of 10 m or less. However, there are compelling reasons that justify obtaining a better knowledge of the deeper sections of these deposits, among others:

1) In almost all cases there is a complete absence of historical record of the mineralogical and geochemical characteristics of the tailings deposited during the years and decades of production, being impossible to anticipate the existence and extent of sedimentation layers with different mineralogical and geochemical characteristics within the different depths of the tailings.

2) Old deposit of tailings (with many years and even decades after their closure) typically generate alteration fronts (e.g., leaching, enrichment and/or depletion of certain elements) that may evolve deep into the deposit of tailings.

3) Depending on the geometry of the tailings deposit, during its deposition the accumulation of heavy minerals in the deeper layers can be favored by gravitational processes, being relatively enriched in heavy metals with respect to the shallower layers. Therefore, a detailed understanding of the deeper sections of the deposit of tailings is essential to understand their geochemical and mineralogical evolution, to generate realistic environmental assessments and to create acceptable economic evaluations for a future revalorization of these secondary deposits.

The main objective of this study, based on detailed and systematic sampling of an IOCG tailings deposit and its geochemical and mineralogical characterization, is to develop geostatistical (using interpolation by co-kriging) and conceptual models allowing to decipher its geochemical and mineralogical spatial-temporal evolution as well as the most relevant physical and chemical parameters controlling this evolution. To this end, the presence of alteration fronts and their possible vertical and horizontal extensions were evaluated. Subsequently, the different factors promoting the alteration of sulfide minerals under arid climate conditions were assessed. In addition, the influence of the deposit geometry and the possible sediments depositional history has been determined. Finally, the environmental implications and possible economic potential of the deposit based on critical raw elements such as Co, REEs, Cu and Fe were considered. This study places special emphasis on the mineralogical and geochemical associations characterizing the final deposit of tailings, together with other relevant physical and chemical parameters (e.g., paste pH, hydraulic conductivity, and particle size distribution).

2. Site description

2.1 Ore geology

The Punta del Cobre district includes the Candelaria deposit, and several medium and small sized mines such as Alcaparrosa, Carola, Las Pintadas, Socavón and Santos, all hosted within volcanic rocks of the Punta del Cobre Formation. These rocks of a pre-upper Valanginian age (Marschik and Fontboté, 2001). Rocks of this formation are subdivided from bottom to top into the Geraldo-Negro Member (> 300 m) and Algarrobo Member (up to > 800 m) comprised mainly of altered sub-aquatic volcanic and volcanoclastic rocks. Mineralization occurs in a diversity of styles including veins, stratiform orebodies, stockworks and hydrothermal breccias, hosted by andesite volcanic, volcanoclastic and volcanic breccia rocks, locally termed an albitophire facies of the Punta del Cobre Formation (Marschik and Fontboté, 2001). Five main alteration types are identified and associated with mineralization as well as a regional contact metamorphism caused by the Coastal Batholith in the western sector. An early episode of hydrothermal alteration generated extensive albitization (albite–quartz–chlorite, ±sericite ±calcite) which was locally superimposed by potassic alteration (K-feldspar–quartz–chlorite/biotite ±sericite ±calcite ±tourmaline). The rest of the alterations are associated with the batholith and are characterized by the following mineral assemblage (from contact, west to east): Ca-amphibole ± biotite ± sericite, biotite ± chlorite ± sericite ± epidote and epidote chlorite ± quartz ± calcite (Marschik and Fontboté, 2001). Main hypogene minerals in the Punta del Cobre District are chalcopyrite, pyrite, magnetite and hematite (Oyarzun et al., 1999).

173 *2.2 Description of the studied mine tailings*

174

175 El Buitre tailings deposit is located in the province of Copiapó, in the community of Tierra
176 Amarilla. The General Directorate of Water of Chile has reported the presence of an unconfined
177 aquifer consisting mainly of an alluvial deposit. The aquifer has been subdivided into 6 sectors
178 to facilitate management of its resources (Fig. S1). El Buitre tailings deposit is located in the
179 vicinity of sector IV, in the lower part of the sub-basin of the Middle Copiapó River, specifically in
180 Los Buitres and Los Diques sub-basins (Compañía Contractual Minera Candelaria, 2013). This
181 region is characterized by an arid climate with an annual average temperature of 18.2 °C and an
182 average annual accumulated rainfall of 22.5 mm/year for the period of 1998-2019. The months
183 of June, July and August present the highest rainfall during the year. The record value in 24
184 hours was 92.3 mm during the month of December 1997, with a return period of 200 years.
185 However, there is a considerable number of years with null precipitation, or that the totality of
186 the annual precipitation was concentrated in one or two days of the year. The averages of
187 maximum, and minimum absolute temperature values in the same period were -0.4 °C and 40
188 °C (Ministerio de Obras Públicas de Chile, 2020). Evaporation rates strongly exceed rainfall
189 (Sistema de información integral de Riego, 2020).

190

191 At present El Buitre tailings deposit is closed, having been in operation from 1997 to 2005
192 and it has a total authorized tonnage of 6.6 Mt. After its closure, it was used until 2010 as an
193 emergency dam, in case the active Las Cruces tailings dam, currently active and belonging to
194 the Pucobre company, presented any inconvenience. Tailings in this deposit are the result of an
195 alkaline flotation circuit (~ pH 10.5-11) designed for the recovery of copper ore concentrates.
196 The plant processed ore deposits from the Punta del Cobre, Mantos del Cobre and Granate
197 Mines, however there are no reliable records regarding which specific mines the ore rock came
198 from. The Punta del Cobre mine extracts copper sulfides and oxides, while the Granate and

Mantos del Cobre mines extract copper sulfides. The deposit of tailings was built by the downstream method, and the tailings were deposited in the form of slurry. According to the historical image of the deposit of tailings (Fig 1a), multiple outfall deposition (spigots) was the deposition method used. At least 3 discharge points are observed along the dam wall in the eastern and central sector of the deposit. In addition, the tailings were not treated with amendments or any remediation technology. However, it has a 30 cm thick layer of coarser tailings fraction (separated by hydrocyclones) on the surface to avoid its dispersion by wind.

3. Samples and methods

3.1 Sampling and fieldworks

All samples were collected in two campaigns during the summer to reduce any heterogeneity caused by climatic conditions. Eight cores up to depths of 4 m were taken with a hand auger, and twenty-four cores at different depths (1-49 m) were taken by sonic drilling. The depth in each core depended on the geometry of the deposit of tailings. Undisturbed samples were obtained by sonic drilling, and color, moisture, grading and degree of alteration and oxidation, with emphasis on sulfide contents were recorded in situ (Fig. 1a). A total of 755 samples were obtained from 1 m sample composites obtained from 755 m of core. These were sealed in plastic bags and stored in ice-packed cooler boxes (8 °C), for later analysis. For the geochemical analysis samples were oven-dried at 30 °C and homogenized in the Mining Sustainability Laboratory of the Chile University.

3.2 Physicochemical parameters

Paste pH was measured according to (Tremblay and Hogan, 2000) using a HI-5222 Hanna pH meter, equipped with a HI-1053B electrode. The pH meter was calibrated every 30 samples with certified standard reference solutions (HI7004L/C and HI7007L/C). In addition, duplicates were analyzed every 10 samples. In addition, particle size distribution of a representative sample composite was performed by Cisa Ro-Tap sieve shaker at ASMIN industrial laboratory, Santiago, Chile. The hydraulic conductivity was measured by a constant-head method for the laminar flow of water through granular soils following the ASTM D2434 procedure. The visual inspection of the drill cores allowed to qualitatively differentiate between the dry and wet tailings samples. This information was used to define a "moisture horizon" that could be defined by the depth at which wet tailings samples are unequivocally identified in each drill core.

3.3 Geochemical methods

3.3.1 Total digestion

The 755 samples collected from 1 m sample composites were completely digested using a 4 acids digestion procedure (HNO_3+HF+$HClO_4$+HCl). A total of 59 elements were measured by ICP/MS (Perkin Elmer Elan, 9000) with detection limits as indicated in Supplementary material, Table S1. One blank was run for every 40 samples, and an in-house control was run every 20 samples. For every 15 samples, a digestion duplicate was analyzed. In addition, digested standards and instrument recalibration were run every 80 samples. All the sample digestions and analyses were performed by Actlabs, an accredited laboratory at Coquimbo, Chile.

3.3.2 Sequential extraction

The sequential extraction was performed by AGQ Laboratories, Santiago, Chile, following the procedure defined by Dold and Fontboté (2001) with the objective to study element speciation in the deposit of tailings. Three boreholes (B-04, B-13 and AD-02) located in the eastern and central sectors were selected with the objective of studying element speciation to the deepest zones of the deposit. A total of 17 composite samples every 2 m were selected from the most superficial, intermediate, and deep zones of the deposit. The depth ranges were selected, taking as criteria mineralogical changes detected from the detailed analysis of the boreholes core and variations in the geochemical data with depth. The first four extractions allowed to separate the mobilized elements and secondary minerals. The last three stages allowed to separate organic material, secondary and primary sulfides, and silicates. For more details on the physical and chemical treatment of the samples and the main dissolved minerals in each step, see Table S2. The solutions were analyzed by Inductively Coupled Plasma Atomic Emission Spectroscopy (ICP-OES) with detection limits indicated in Table S3. Saturation index (SI = logIAP – logK; IAP = ion activity product) of gypsum with respect to water soluble fraction element concentrations were calculated using PHREEQC version 3.6.2-15100 and the paste pH value was used as a reference.

3.4 Mineral characterization methods

A total of 340 composite samples every 1 m were analyzed by X-ray diffraction (XRD). Samples located in the closest and most distal zone of the dam wall, and in the central zone of the deposit of tailings were analyzed. In addition, samples belonging to different depth ranges were selected, taking as criteria mineralogical changes detected from the detailed analysis of

the boreholes core and variations in the geochemical data with depth. These selection criteria were also used for all other mineralogical analyzes. Homogenization and micronisation of the tailing's particles were carried out to obtain grain sizes of less than 10 microns. The mineralogical composition was determined using a Bruker® D8 Endeavor X-ray diffractometer with a tube with cobalt radiation. Diffractometer settings were: 35 kV, 40 mA and a scan range of 3–70° 2θ, 0.02° 2θ step size, and 5 s counting time per step. The obtained diffractograms were analyzed using the software DIFFRAC. EVA® version 4.2 and DIFFRAC.TOPAS® version 5.0. The Powder Diffraction File™ (PDF-2 2001) database was used for phase identification. Spectra standard of corundum was used for semi-quantification of mineral phases. Besides, QA/QC was performed by analysis of duplicates and X-ray fluorescence. In addition, clay minerals from 202 composite samples every 1 m were characterized following USGS protocol (USGS, 2000). The < 2 µm fraction was separated by centrifugation and the samples were analyzed by XRD before and after heat treatment. The semi-quantification of clays was carried out with spectra standards of montmorillonite, kaolinite and illite. XRD analyzes were performed by Geomaq Limitada, an accredited laboratory at Antofagasta, Chile.

A total of 100 composite samples every 1 m were prepared in polished thin sections and analyzed by optical microscopy Olympus model BX51, using reflected-light mode to identify opaque minerals in the tailings assemblage. The mineral composition was determined by the count point method at 350 equally spaced points across the thin sections. In addition, photomicrographs were obtained to complement the observations. This analysis was made in the Minerals Laboratory of the Mining Department of the Chile University. In addition, semi-quantitative element composition was studied by Quantitative Evaluation of Materials by Scanning Electron Microscopy (QEMSCAN) combining information generated by the retro dispersed electrons (for imaging) and X-ray dispersive energy spectra (EDS) for chemical composition. A total of 150 composite samples every 1 m were analyzed. The Bulk Mineral

299 Analysis (BMA) measurement method was used to provide statistically abundant data for
300 mineral identification, speciation, distribution, and quantification. This analysis was performed by
301 SGS minerals, Chile.
302
303 *3.5 Statistical methods and geostatistical modelling*
304
305 The database of total digestion and sequential extraction was filtered and adjusted according
306 to the following criteria. 1) All the values below the detection limit (LOD) were changed
307 according to the values resulting from dividing the specific detection limit value by the square
308 root of 2 (Hites, 2019). 2) Variables with more than 50 % of data under the LOD was not
309 suitable to be included in any statistical analysis and was eliminated. 3) The normality of the
310 data was evaluated by the Kolmogorov-Smirnov tests. Due to the non-normal distribution of the
311 dataset, the transformation to normal logarithm was performed. 4) Alpha was set at 0.05 for
312 interactions. The mean value of chemical data (as the dependent variable) concerning different
313 depths was analyzed using one-way factorial ANOVA and Welch t-test. Tukey's and Dunnett
314 T3's multiple comparisons procedures by homogeneous and non-homogeneous variables were
315 performed.
316
317 A Principal component analysis (PCA) was carried out by means of a Pearson's correlation
318 matrix (0.05 significance level, 2-tailed test) on all validated variables in order to define the main
319 element associations and the reflected mineralogical variations, for the interpretation of
320 processes such as weathering or to characterize variations of origin. This analysis is also used
321 to interpret these associations in terms of geochemical processes by comparing their patterns
322 with other analytical determinations (sequential extraction, mineralogical characterization, and
323 geostatistical model). PCA discovers linear combinations of the variables based on measures of
324 association and, it allows the reduction of dimensions for a complex multi-element dataset. The

results are graphed in a biplot. It is a plot of the PC loadings for each variable with the loadings of each sample along two sets of PC axes (Abraitis et al., 2004). Evaluation of the chemical data, PCA analysis and one-way ANOVA was performed using ioGAS 7.3 and IBM SPSS Statistics 25 software, respectively.

The estimation of the grades in the deposit of tailings was carried out using interpolation by cokriging. This method allows modelling the grades in the deposit based on drill core depths and considering together all the grades of the study and the spatial continuity through variographic analysis. Due to the lack of information of the previous underlying topography the tailings, the tailings bottom surface was modeled by kriging the length of the drill cores at the studied domain. The estimation of the bottom surface was performed as follows: 1. the bottom surface was defined to estimate the total volume of the restricted modeled area (Kokkola, 1986); 2. the bottom surface of the whole the deposit of tailings was restricted by the dam structure, to estimate the total volume of the deposit (Parviainen, 2009). The total resources of Co, Cu, light rare earth elements (LREE), heavy rare earth elements (HREE), Fe, S, Ca, P and Al were estimated using a 3D block model and a discretization cell of 3 m x 3 m x 2m (Deutsch and Journel, 1997). This model was arranged according to a sampling grid with horizontal distances of five meters and depth intervals of one meter (block size of 5 m x 5 m x 1 m) resulting in a total of 1,800,000 blocks. The validation of the models was carried out by cross validation with the chemical data. The modelling workflow was performed by the method proposed in (Parviainen et al., 2020). This methodology takes into consideration the difficulties in defining the topography of the abandoned tailings and the anisotropy generated by the greater length of the horizontal direction than the vertical direction. Multivariate modelling was performed using the ANDES software (Soto et al., 2017).

4. Results and Discussion

4.1 Tailings morphology and physical and hydraulic main characteristics

Modelling the tailings' depth and current surface topography is very important to properly estimate the tailings precise volume for future revalorization and reprocessing studies. It is also important to control the physical stability of a future operation because it will control the formation of a ditch network eroding the tailings surface (Parviainen et al., 2020). The thickness of the deposit of tailings was determined from the drill holes, taking into consideration that the surface topography was quite regular, and the deepest areas were delimited by coarse sand and gravel and by a waterproof membrane of high-density polyethylene in the area the dam wall. The deposit's thickness varies from one to 49 m. The deepest parts of the tailings are in the eastern and central parts of the deposit of tailings (Fig. 1b), following the original shape of the valley basin where the tailings were deposited. In the western area, the depth tends to decrease, ranging from 1 to 25 m (Fig. 1b). From a sedimentary perspective, visual field observations showed that the tailings deposit is comprised by alternating fine sandy to clayey-silty layers. Particle size analyses of a composite sample from one drill hole showed that the cumulative passing curve is ranging from 1 to 300 µm, and d*80* is 40 µm (Fig. S2 a and b). This distribution of particle size is in agreement with the milling stages required for the flotation process in tailings with similar characteristics (Medina et al., 2019). Please notice that, although this grain size distribution curve can be useful for a general understanding of the tailings deposit, it does not provide detailed information about the grain size distribution within the specific horizontal layers observed along the tailings depth profile. The proportion of sand and clay changes with borehole depths and with their locations respect the dam wall. The first five meters of depth are typically more sandy, whereas the intermediate zone (5-17 m) presents intercalations of sand-clay-sized material, and the deepest zone (> 17 m) is mainly clayey (Fig.

1c). This particle size distribution has a direct impact on the hydraulic conductivity of the deposit of tailings (Fig. 1c), resulting on low hydraulic conductivity $K = 1.3 \times 10^{-6}$ cm/s for the deepest layer and higher hydraulic conductivities (in the order of 10^{-4} cm/s) for the more surficial layers (0-17 m). To illustrate the distribution of the moisture horizon within the deposit of tailings, an iso-piezometric map was made. It shows how this horizon is deeper towards the central sector of the deposit of tailings, in the area more distal to the streams located northeast and northwest of the deposit of tailings (Fig. S3). On the other hand, the moisture content within the deposit of tailings appears not to be influenced by the presence of groundwater. According to groundwater level monitoring and quality control wells located in El Buitre sector (Fig. S1), the confined aquifer is found at a depth greater than 125 m (the maximum tailings depth is 49 m). Besides, the Alcaparrosa well located in the vicinity of El Buitre sector, has diminished by 40 m in the period 1998-2008, as a result of agricultural activities in the area. Additionally, the recharge of the aquifer by natural processes is complex, since the potential evaporation considerably exceeds the precipitation, causing the net recharge to tend to zero. Therefore, groundwater recharge occurs during wet years. According to the record of the last 40 years of the Copiapó Weather Station (1971-2011), it is estimated that the recharge is between 5 to 12 mm/year (considering a recharge rate of 10 %) (Compañía Contractual Minera Candelaria, 2013).

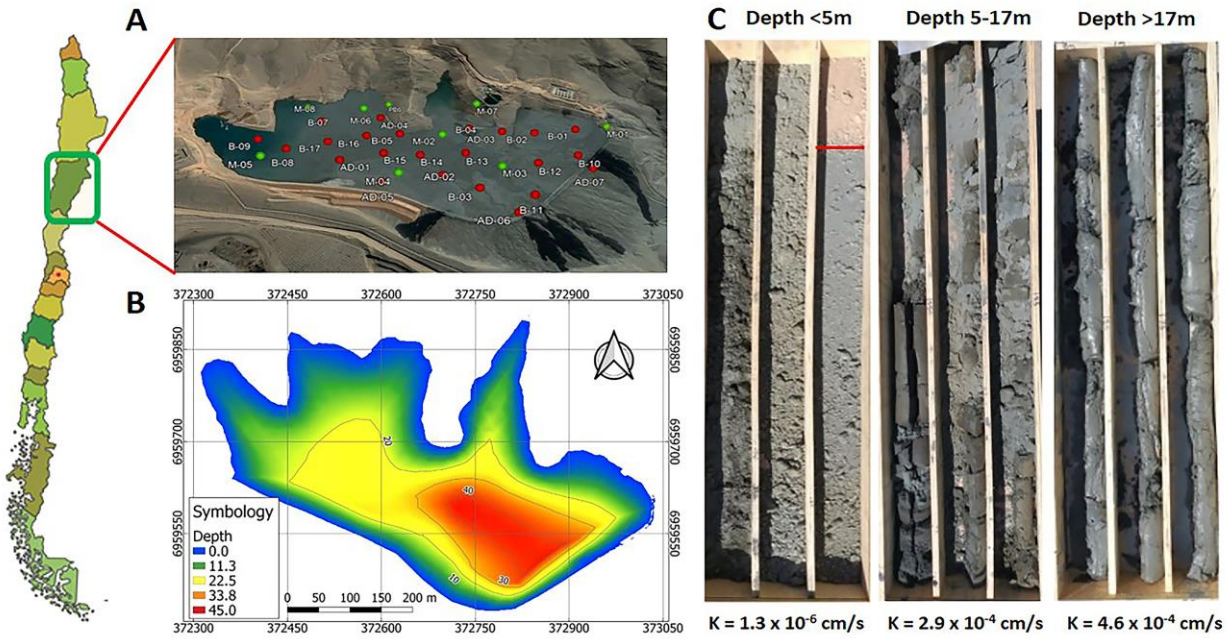

Fig. 1. *a)* Historical satellite image (2004) showing tailings discharge points and the location of the boreholes (red spots = sonic drilling and green spots = hand auger); b) depth spatial variation within the deposit of tailings; c) representative tailings core sample boxes of different depth ranges. The first box on the right shows a light brown layer that corresponds to coarse tailings fractions used to avoid wind borne dispersion.

4.2 Mineralogical characterization

The mineralogical composition of the tailings is quite homogeneous, most samples are similar in mineral composition and abundance. XRD shows that quartz, chlorite, alkali-feldspar (microcline and orthoclase), plagioclase and magnetite are the main mineral constituents, whereas other minerals like hematite, calcite, pyrite, and gypsum-anhydrite appears as minor mineral constituents of the deposit of tailings (Fig. 2 and Fig. S4). Illite, chlorite, and kaolinite were the typical minerals in the clay fraction <2 µm. Additionally, QEMSCAN analyses (more reliable than XRD analyses for minerals with wt % lower than 1 %) show that muscovite, biotite, tourmaline, rutile, apatite, amphibole, sphene, pyroxenes, ilmenite, epidote, dolomite/ankerite

and garnet could be considered as trace constituents (Table S4). Also, the QEMSCAN study revealed that chalcopyrite is the main Cu-bearing mineral (ranging from 0.163 wt % to 0.02 wt %), whereas other minerals like chalcocite/digenite, enargite/tennantite and malachite/azurite can be considered negligeable, with and abundance lower than 0,0001 wt % (Fig. S5).

The relative abundance of magnetite (Fig. 2b), orthoclase and microcline (Fig. S4 c and h) do not significantly change with depth. Therefore, they are homogeneously distributed in the deposit of tailings and alkaline-feldspar probably does not act as neutralizing agent. In contrast, pyrite and calcite (Fig. 2a and 2e) progressively increase their abundance with depth, moving from values around 1.5 wt % and 2.5 wt % on the tailings surface to values around 3.5 wt % and 7.5 wt % in the deepest layer, respectively. This trend might be the result of pyrite oxidative leaching and acidity generation at the most surficial part of the tailings (where scarce rainwater reaches) followed by calcite dissolution and leaching solution neutralization. In accordance with that, the tailings showed a mean paste pH of 7.9, with values consistently ranging from 7.78 to 7.95 (Fig. S2c). On the other hand, the gypsum content remains practically constant with depth, however, it decreases significantly in the depth range of 12-14 m. (Fig. 2d). This gypsum distribution is in accordance with aforementioned pyrite oxidation and leaching process and neutralization of acid solutions by calcite. Apatite shows relative abundances significatively higher for the deeper samples (in the range of depths of 6-10 m and 12-14 m) than the shallower samples (Fig. 2c). This distribution could be attributed to the gravitational deposition of apatite particles in the deposit of tailings.

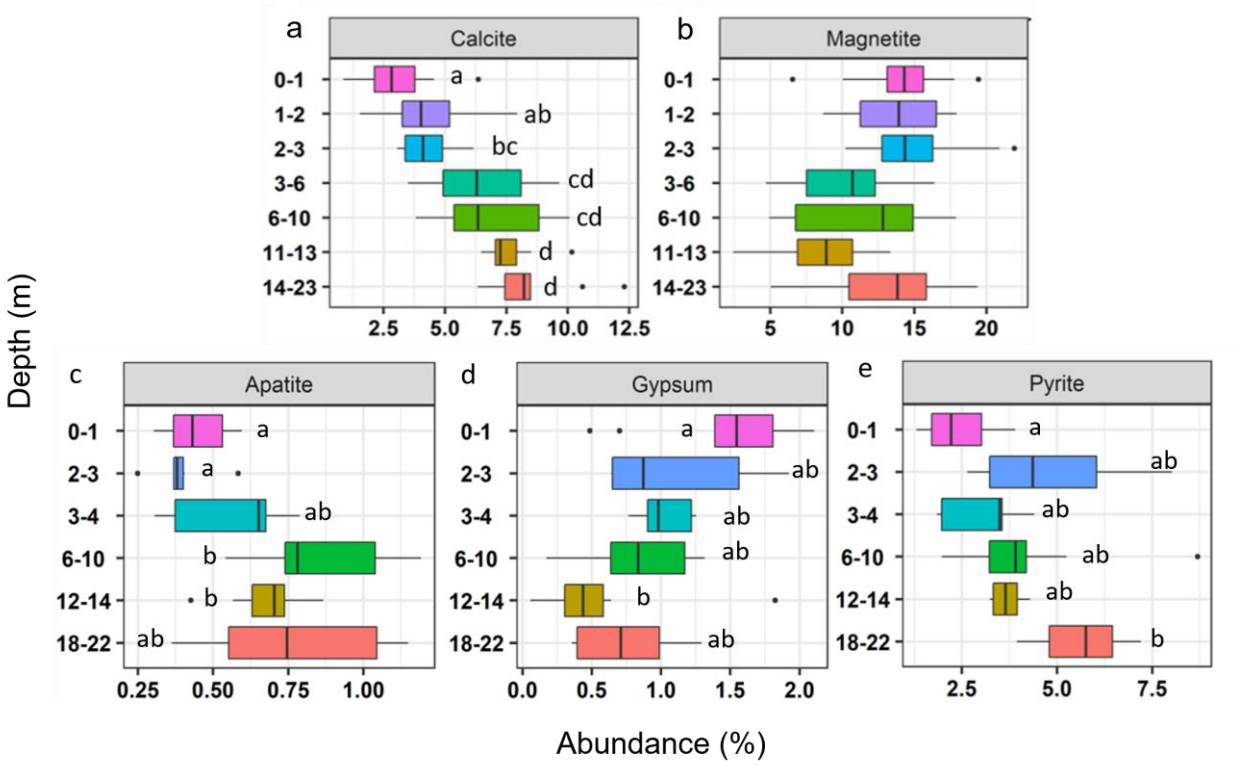

Fig. 2. Mineralogical characterization of major minerals (calcite and magnetite) by XRD (340 samples) and minority minerals (pyrite, gypsum, and apatite) by QEMSCAN (150 samples) in samples at different depths. The lowercase letters on the graph represent a one-way ANOVA analysis. Different letters indicate that there is a significant difference between the relative abundance of the mineral at a certain depth. On the contrary, the same letters indicate that there are no significant differences. Minerals without letters indicate that the relative abundance of the mineral does not present significant differences in any of the analyzed depths.

Complementary to the XRD study, the examination of polished sections showed that the sulfide assemblage is dominated by pyrite (ranging from 1.2 to 8.7 wt %), which is little fractured and disturbed in the oxidation zone, not showing Fe (III) oxyhydroxides rims or coatings (Fig. 3a). Low alteration of the sulfide assemblage in neutral tailings has been reported by Dold and Fontboté, 2002; Lindsay et al., 2009b. Chalcopyrite and sphalerite are present as trace minerals and do not show replacements. Chalcopyrite is associated with magnetite, sphalerite, and pyrite

(Fig. 3a and f). Supergene Cu-sulfide were not identified by petrographic microscopy and QEMSCAN analysis indicated that these minerals are below 0.0001 % in abundance. The oxide assemblage is dominated by magnetite and hematite, and trace amounts of specularite, goethite, and ilmenite. Hematite in the form of specularite has been described by Marschik and Fontboté (2001). Magnetite is partially replaced by hematite (Fig. 3c) and goethite at the edges and fractures, and hematite is partly replaced by goethite. In addition, magnetite is commonly associated with ilmenite, hematite, and chalcopyrite (Fig. 3b, e, and f). The replacement of magnetite and hematite by goethite at the edges can occur for oxidation reactions in the deposit of tailings. On the contrary, the pervasive magnetite alteration to hematite and magnetite and hematite alteration to goethite (Fig. 3c and d) can be attributed to hydrothermal alteration processes within the deposit of origin.

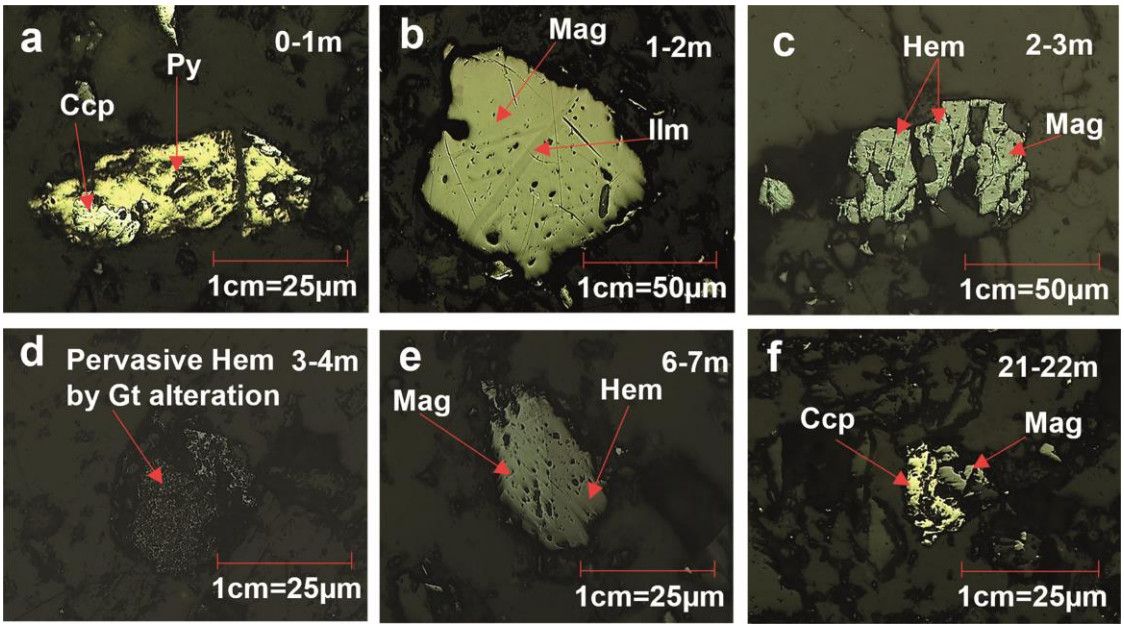

Fig. 3. Mineralogical characterization by petrographic microscope in samples with different depths. A) Pyrite-Chalcopyrite (Py-CCp) association, b) Magnetite (Mag) with ilmenite (Ilm) bands, c) Mag partially replaced by Hematite (Hem) at the edges and fractures, d) Pervasive Hem by Goethite (Gt) alteration, e) Mag-Hem association and f) CCp-Mag association.

4.3 Geochemical and Geostatistical characterization

The original database of 59 elements (Table S5) was reduced to the 31 elements presented in

Table 1. In addition to the previous filters carried out before the statistical analysis, some immobile elements with very low concentrations were eliminated (Ba, Cd, Cr, Hg, Hf, Nb, Rb, Sb, Se, Sr, Ta, Te, Tl, Zr). REEs was divided into LREE and HREE to improve the visualization of the data distribution patterns and because of the very different commercial value of both groups. Table 1 summarizes the geochemical composition and the univariate statistics of the tailings. As expected from its mineralogical composition, the bulk chemistry of the tailings is mainly comprised of Fe, Si, Al, Ca, S and P, which is in accordance with the geochemical analyses of similar IOCG deposits in this region (Medina et al., 2019; Sernageomin, 2020b).

Taking as reference grades reported for ore deposits and deposits of tailings worldwide, it is possible to indicate a significant content of some value elements e.g., Co (103 ± 32 mg/kg), Cu (795 ± 514 mg/kg), and REEs (337 ± 118 mg/kg). In addition, it is necessary to take into consideration that due to the energy and infrastructure savings associated with the reprocessing of tailings, it is possible to exploit lower elemental ore grades (Parviainen et al., 2020). Mud and Jowitt (2018) reported Cu grades from 0.18 to 1.5 wt % in ore deposits around the World. While economic recovery of Cu has been reported in Minera Valle Central (Rancagua, Chile), a company that reprocesses fresh tailings from El Teniente mine and old mine tailings from the Cauquenes tailings deposit with Cu grades from 0.1 wt % - 0.25 wt % (Henderson, 2018). Regarding Co grades of ore deposits around the World, Mudd et al., (2013) reported values ranging from 0.019 to 0.24 wt %. While in the case of REEs, deposits ion adsorption clays contain REOs from 0.02-1 % (Su, 2009). On the other hand, some pollutants elements e.g., As (38 ± 12 mg/kg) and Pb (12 ± 6 mg/kg) are present in considerable concentrations in the solid fraction and their solubilization could represent an environmental risk.

A geostatistical model (using a 5 m x 5 m x 1 m block model, a total of 1,800,000 blocks) was made to facilitate the interpretation and visualization (3D) of the bulk chemistry spatial variations within the tailings (Fig. 4 and Fig. S6). In addition, it allowed to evaluate the tailings as a "secondary ore deposit", by modeling some critical elements, e.g., Cu, LREE, HREE and Co (Fig. 4). Variographic analysis and validations of the model can be found in Fig. S7 and Fig. S8.

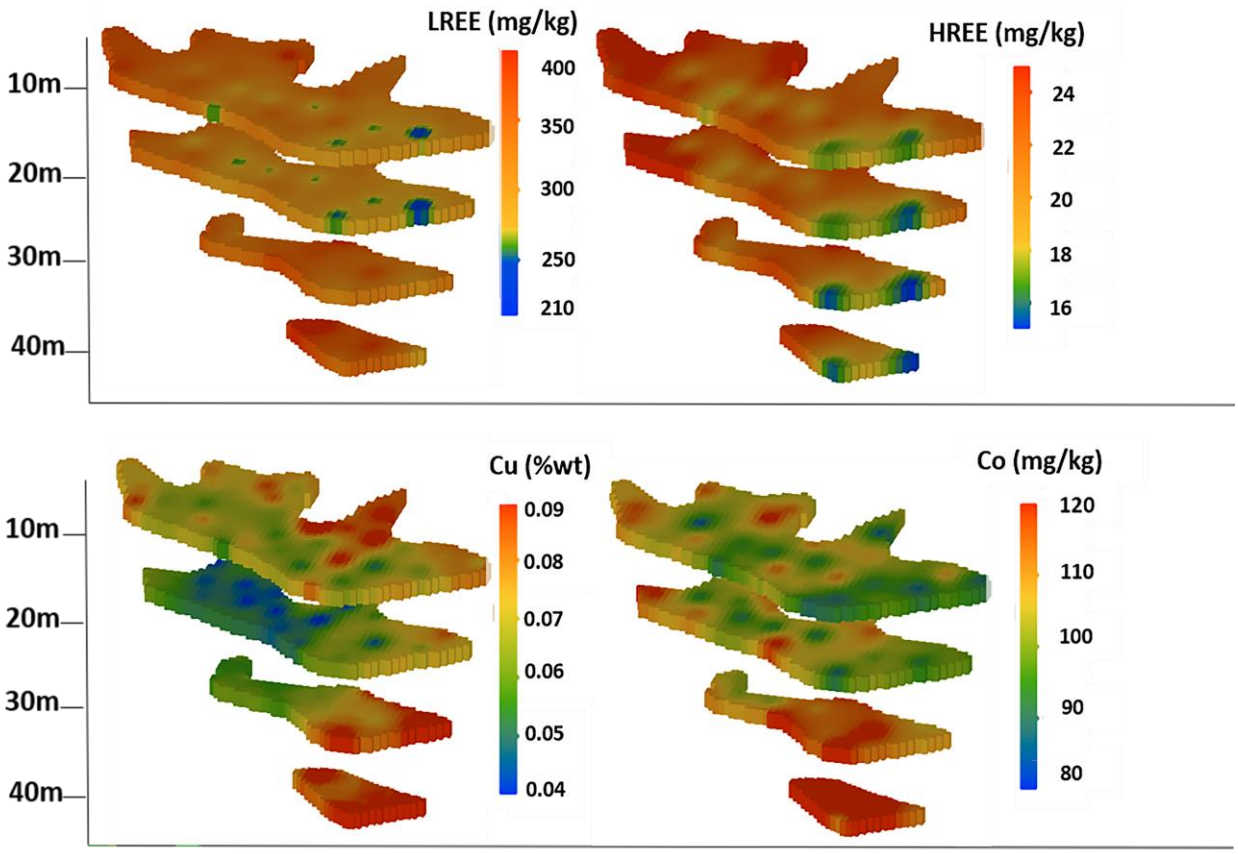

Fig. 4. Spatial distribution of LREE, HREE, Cu and Co grades in the deposit of tailings according to the block model. All 3D views were separated into sections at every 10 m depths to facilitate data visualization.

Based on the block model, some general trends for the mineral forming elements can be observed. The Fe concentrations distinctly increases from West to East and from top to bottom

(Fig. S6). On the other hand, Al and Ca concentrations tend to decrease from West to East in all depths, clearly displaying the lowest concentrations at the dam wall proximity (Fig. S6). Sulfur, and phosphate to a lower extent, show a tendency to increase with depth (Fig. S6). Regarding the modelled grades for some selected critical elements (Fig. 4), a modelled mean grade for LREE of 324 mg/kg (ranging from 209.1 to 524.2 mg/kg) was obtained. Some enriched layers (> 350 mg/kg) can be observed in the central and western sectors at all depths. However, the tailing's LREE concentration can be considered relatively homogeneous. On the other hand, HREE modelled mean grade is 21.5 mg/kg, ranging from 14.6 to 29.1 mg/kg, showing more significant grades increase on an east-western direction in all depths. Modelled Cu mean grade is 0.069 wt %, ranging from 0.037 to 0.157 wt %. The highest concentrations are found in the eastern sector at 30 m and at the bottom of the tailings (depth > 40 m, Fig. 4). Finally, the modelled Co mean grade is 105 mg/kg (Fig. 4), ranging from 79 mg/kg to 171 mg/kg, and clearly showing higher grades in the deepest levels (> 30 m).

It is important to take into account that the present geostatistical model is based on chemical data obtained from a high density sampling campaign (32 boreholes) that were drilled to the bottom of the deposit. This allows a reliable estimation of the grades and geometry of the deposit. Therefore, the results of the present study can be considered an excellent exploratory model to evaluate the economic potential of this waste. Based on the mean grades of the elements of interest and the lowest reported cut-off grades for tailings and deposits worldwide, a rough estimation of the total remaining resources for Cu, Co and REEs (Table 2) using the volume of the whole the deposit of tailings was made. It was considered a tonnage of 6.6 Mt (Sernageomin, 2021a). Additionally, Fe was included, because currently the Compañía Minera del Pacífico (Copiapó, Chile) produces pellet feed with tailings from the copper concentrator plant of the Compañía Contractual Minera Candelaria, with average Fe grades of 11.4 % (Compañía Minera del Pacífico, 2020). According to this estimate, the modeled mean

concentrations of Fe and REEs present 100 % of the blocks above the cut-off grade (11.4 wt % and 0.02 wt %) and they represent 1.023 Mt and 0.00132 Mt of the reserve (Fig.S9). The modeled mean concentrations of Cu present an estimated 2.1 % of the blocks are profitable, with grades above the cut-off grade (0.10 wt %). While the average modeled concentrations of Co show 100 % of the blocks below the cut-off grade (0.19 wt %) (Fig S9). On the other hand, economic potential was calculated as the fraction of each value element in the tailings multiplied by the mass of the deposit and the metal price (Table 2). The price of REEs was 4,651,315 US/ton and it corresponds to the average of Eu_2O_3, Gd, Tb, Dy, Er, Y, La, Ce, Pr, Nd, Sm.

The results indicate a high economic potential for iron and REEs. In contrast, Cu and Co represent a low potential, because the modeled average grades are below the reference cut-off grades (Table 2). Parviainen et al, (2020) suggest considering tailings deposits as polymetallic deposits to increase their economic potential. However, the revaluation of tailings depends on other factors like metal price, element-bearing mineralogy for elements of interest, metallurgical recovery technologies, dimensions of the deposit of tailings (allowing scale economy), OPEX and CAPEX costs (Araya et al., 2020, Parviainen et al., 2020; Araya et al., 2021), among many other considerations. El Buitre tailings deposit can be considered small (6.6 Mt), which could limit its profitability. Nevertheless, adjacent to its location, there are other tailings deposits belonging to the Pucobre company, with similar characteristics, that could be reprocessed together. Currently, the Compañía Minera del Pacífico extracts 3.5 Mton/year of Fe by magnetic separation from the deposit of tailings belonging to the Compañía Contractual Minera Candelaria. It has the potential to reprocess deposits of tailings located nearby, including El Buitre tailings deposit. Additionally, during the cleaning process and concentration of magnetic Fe could concentrate pyrite, chalcopyrite and apatite, therefore the extraction of Cu, Co and REEs as secondary products could be favored. The Compañía Minera Valle Central extracts Cu from tailings by froth flotation. Meanwhile, the Co associated with pyrite has been extracted by

555 bioxidation-flotation and bioleaching of sulfidic tailings of iron mines (Ahmadi et al., 2015;
556 Parbhakar-Fox et al., 2018). On the other hand, the possible association of REEs at different
557 mineral phases e.g., phyllosilicates and apatites, could hinder their extraction. Araya et al.,
558 (2020) conducted a techno-economic feasibility study of industrial-scale REEs recovery from
559 copper industry tailings, proposing chloride-based hydrometallurgical extraction technology
560 processes as a potential alternative to traditional capital intensive hydrometallurgical processes
561 based on high temperature and pressure (Onyedika et al., 2012). The study was carried out in
562 Chilean tailings deposits with characteristics similar to El Buitre. They determined a net present
563 value (NPV) to 20 years (income that an investment will generate in the future) of 672,987 USD,
564 exceeding the initial investment cost taken as a reference (342,514,448 US$). In addition, the
565 internal rate of return (IRR) that refers to the discount rate at which the NPV of future cash flows
566 is equal to the initial investment, was 10.03 %. It was almost the same as the discount rate
567 chosen for the project (10 %), indicating that the project was not highly profitable. Nevertheless,
568 these calculations considered the average price of REEs of 22 US/kg for the year 2018,
569 including cerium, lanthanum, samarium, gadolinium, praseodymium, dysprosium, and yttrium
570 oxides. Additionally, they projected for the year 2022 an increase of 23 US/kg. However,
571 currently the average price of REEs in element form is 4651.31 US/kg, including Eu, Tb and Nd.
572 Therefore, the extraction of REEs can currently be considered viable taking as a reference the
573 COPEX, OPEX, production capacity and discount rate proposed by Araya et al., 2020.

574 *4.4 Multivariate Statistical Analyses*

575

576 Total digestion geochemistry results were studied using the PCA statistical method to define
577 elemental and mineralogical associations as well as to observe possible weathering/ alteration/
578 depositional processes. Samples were split into the HREE groups (< 5 m, 5-17 m and > 17 m
579 depth) and submitted to the PCA study. This differentiation was made based on the trends of

the concentrations obtained by total digestion of Cu, Co, S and Fe, and changes in the mineralogical composition (pyrite, apatite and calcite) along the depth profile (Fig. S10 and Fig. 2). As can be observed in Fig. 5 (left panel) 43.8 % of the variance of the samples from 0 to 5 m depth are explained by two components. The first principal component (PC1) is by far the predominant one and accounts for 28.33 % of the variance, while the second one (PC2) only explains 15.47 %. PC1 is related to silicate minerals, mainly aluminosilicate of Mg, Ca, and Mn, as well as to immobile elements like Cs, Ga, Be, Li, Sn, U, Ag, Co, Ni, Th, Zn and HREE. A Pearson's correlation matrix (Fig. S13) shows that Al exhibits a good positive correlation with HREE (0.651) but no correlation with LREE (0.319). This could be attributed to the adsorption of HREE on micas under the neutral or low pH conditions of the tailings deposit. Yang et al., (2019) indicate that at low ionic strength the adsorption of REEs on kaolinite and halloysite increases with increasing pH conditions. The second principal component could be attributed to the higher presence of sulfide minerals in these surficial samples, as shown by the high loading shown for S (-0.844). The cluster of elements close to Fe (i.e., As, Bi, Co and Ni) are clearly related to the presence of pyrite in the deposit of tailings. A Pearson's correlation matrix shows that S exhibits a strong positive correlation with Ni (0.709) and Co (0.817) and a good positive correlation (> 0.5) with Fe, Ag, As, and Bi, supporting the previous interpretation (Fig. S13). Pyrite is the most abundant sulfide in the deposit of tailings, a mineral that can incorporate these elements within its crystal structure (Abraitis et al., 2004; Moncur et al., 2005; Paktunc et al., 2006; Deditius et al., 2011).

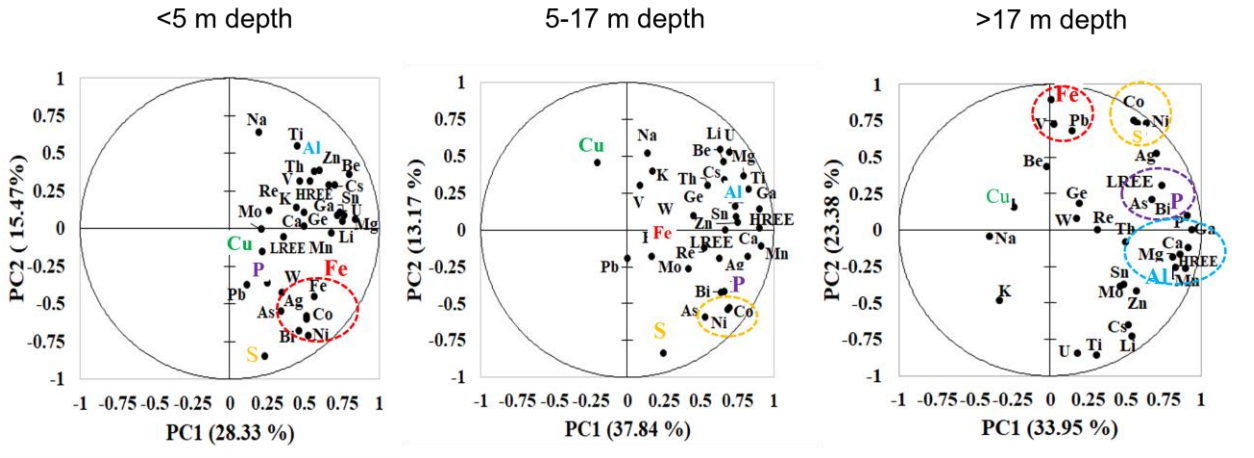

Fig. 5. Principal Component Analyses for tailings samples with depths < 5 m, between 5-17 m and > 17 m.

The PCA from samples with depths in the range of 5-17 m are shown in Fig. 5 second panel. As can be observed, 51.01 % of the sample's variance can be represented by two components (PC1 37.84 % and PC2 13.17 %). As in the most surficial samples, the first principal component could be related to Mg, Ca, and Mn aluminum-silicate minerals, as well as associated to immobile elements whereas the second main component could be attributed to the presence of sulfide minerals, mainly pyrite. However, the elements clustering and the interpretations assigned to this second set of samples are not as evident and robust as for the most surficial samples. Finally, the PCA from samples with depths higher than 17 m are shown in Fig. 5 third panel. As can be observed, 57.3 % of variance can be represented by two components (PC1 33.95 % and PC2 23.38 %). At least four different element clusters were identified in this PCA. The first principal component is associated with elements that cluster around P and LREE (attributed to the presence of apatite in the tailings) and a cluster that associates with Al (Ca, Mg, Mn and HREE) that likely reflect the silicate minerals in the tailings. A Pearson's correlation matrix shows that P exhibits a strong positive correlation with HREE (0.800) and LREE (0.697)

(Fig. S13). However, HREE also show a very good Pearson's correlation with Al (0.834). Therefore, in the deeper samples the HREE and LREE could be incorporated into the crystalline structure of apatite as well as in other silicate minerals. The association of elements in the second principal component determines a cluster around S (Ni and Co), most probably reflecting the presence of pyrite. A Pearson's correlation matrix (Fig. S13) shows that S exhibits a strong positive correlation with Co (0.921), Ni (0.919) as well as with Ag (0.824). A second cluster around Fe is also evident for PC2, with V and Pb showing high positive loadings. According to a Pearson's correlation matrix, Fe exhibits a strong positive correlation with V (0.740) and a good correlation with Pb (0.507). This cluster can be attributed to the presence of magnetite and hematite within the tailings deposit. The positive correlation with Pb and V could be attributed to the adsorption of these metals on Fe (III) oxides (Liang et al., 2017).

Based on the main elements grouped by the PCA, one-way ANOVA and Welch test analyses were carried out in order to determine significant differences among the element concentrations in the three studied depth ranges (i.e., < 5 m, 5-17 m and > 17 m; Fig. S11). The results from this study are clearly in good agreement with previous mineralogical and geochemical observations:

1) Al (linked to the presence of aluminosilicates) and HREE concentrations are significantly lower in the deeper levels (> 17 m);

2) P concentrations are significantly lower in surficial samples (< 5 m depth), however, the lowest concentrations of LREE correspond to the samples located between 5-17 m depth;

3) S and Cu concentrations are significantly higher in the deeper levels (> 17 m depth) in accordance with the higher relative abundance of pyrite in deeper samples;

4) Fe (and V) concentrations do not show any significant difference among the three depth groups, as it would be expected from the homogeneous distribution of the major oxides (magnetite and hematite, Fig. 2) in the deposit of tailings.

One way ANOVA and Welch test analysis were also used to determine statistically significant differences among the horizontal elemental concentrations. To this end, the samples were grouped according to their presence in the eastern, central, and western sectors of the deposit of tailings (Fig. S12). The results can be summarized as follows: 1) Al, REEs, P and Ca concentrations are significantly higher in samples located in the western sector; 2) Fe, Cu, and Pb concentrations are significantly higher in samples located in the eastern sector. The concentrations of the second group of elements increase in the opposite direction than the first group. These trends are in accordance with the mineralogical characterization, and they could be attributed to a gravitational segregation process during deposition and accumulation. As it occurs in most mine tailings deposits (Pan et al., 2014) minerals with higher specific gravities (like sulfides and Fe-oxides) tend to settle down in the area closest to the dam wall (where the tailings discharge is produced) whereas minerals with lower specific gravities (like aluminosilicates) typically reach the most distal areas of the deposit.

4.5 Sequential extraction

A mineral sequential extraction procedure (SEP) was implemented as an additional tool linking the observed mineralogy and bulk chemistry and to generate a better understanding of elemental mobility within the tailings profile. The methodology of seven steps developed by Dold and Fontboté (2001) was used. This procedure was optimized for IOCG-type tailings deposits located in the vicinity of the study area and with similar mineralogical composition to El Buitre tailings deposit.

669 The SEP results obtained from three selected boreholes (i.e., B-04, B-13, and AD-02) were
670 averaged to have a representative value for each depth (Table 3). Taking into consideration the
671 mineralogical and geochemical information previously presented, as well as the multivariate
672 statistical analysis, the following elements were selected to study the selective dissolution of the
673 most relevant minerals in the tailings deposit: 1) Al and Mg, as indicators of primary silicate
674 minerals; 2) Ca, as indicator of carbonates and gypsum; 3) S, as indicator of sulfide and sulfate
675 minerals, 4) Cu, as indicators of chalcopyrite and 5) Fe, as indicator of Fe (III) oxides, Fe (III)
676 oxyhydroxide and sulfides. Other elements were also studied to characterize the mobility of
677 potential pollutants (i.e., As, Mn, Cr and Ni) and critical raw elements (i.e., V and Co) within the
678 tailings deposit.
679
680 The aluminosilicates (marked by the combined presence of Al and Mg) are mostly dissolved
681 in the very last step of the SEP (i.e., Step 7: residual fraction), and they did not show any
682 discernible trend along the depth profile. Gypsum distribution, marked by Ca and S release
683 during the first step of the SEP (Ca/S molar = 1 in Step 1), did not show significant differences
684 through the depth profile (Table 3). In addition, the saturation index calculated using PHREEQC
685 corroborates the precipitation of gypsum by saturation, product of pyrite and calcite dissolution
686 in oxidizing conditions (Table S7). Calcite dissolution can be traced by Ca release, mostly
687 limited to the second step of the SEP (exchangeable fraction and carbonates). As shown in Fig.
688 6, calcite concentration progressively increases with depth. Mn is also predominantly released
689 during Step 2, following a similar distribution as the one described for Ca. In addition, a Pearson
690 'correlation (Fig. S13) shows a strong correlation between Mn and Ca for samples <5 m (0.803),
691 in the range from 5-17 m (0.909) and >17 m (0.915). Regarding the sulfide minerals, it can be
692 observed how sulfur is predominantly released in step 5, and to a lesser extent in step 6, as
693 opposed to what could be expected from the optical mineralogical study that presented
694 secondary Cu sulfide as a minor sulfide and pyrite as major sulfide phase. Dold and Fontboté

(2001) already observed this type of inconsistencies in other mine tailings and they attributed it to the presence of unstable pyrite minerals from the oxidation zone that may partially dissolved in the fifth step of the SEP. Notwithstanding, almost no S reached Step 7, so sulfide selective dissolution was achieved between Steps 5 and 6. Combining Steps 5 and 6, it can be observed how sulfide concentrations slightly increases with depth (Table 3), in accordance with previous mineralogical observations (Fig. 2). Cu concentration (adding all the steps) decreases from the surface to the center of the tailings deposit to finally increase again in the deepest levels, in accordance with previous observations (Fig. 4). Finally, Fe (III) oxyhydroxides and Fe (III) oxides should be selectively dissolved in the third and fourth step of the SEP. However, most of the Fe and its associated elements (V and Cr) were predominantly released (Table 3 and S6) in the last step of the SEP (residual fraction). This discrepancy could be explained because the solubility of Fe oxides is highly dependent on crystallinity. Highly crystalline Fe (III) oxides remain practically unchanged (and their Fe is not released) until the last step of the SEP (Caraballo et al., 2018).

According to the Chilean Norm 46/2002 for the emission of liquid waste into groundwater in highly vulnerable environments, the concentrations of As and Ni were found in low concentrations (Ministerio Secretaría General de la Presidencia de Chile, 2002). In addition, these elements remain mostly immobile until the last steps of the SEP (Table S6), when pyrite is dissolved. On the other hand, Mn is more mobile, and it is significantly released in step 2, during the neutralization reactions induced by calcite dissolution (Table S6). Finally, V and Cr show very limited mobility (Table S6) that is coupled to the dissolution of the Fe oxides (i.e., hematite and magnetite).

5. Conceptual model

In the deposit of tailings it is possible to distinguish geochemical and mineralogical variations with increasing depth and in the area distal to the wall dam or the waste discharge zone. The presence of multiple discharge points and the geometry of the deposit, favor the stratification of the tailings due to coarse particle segregation and settling near the spigotting points. Additionally, tailings stratification may be associated with mineralogical changes, and process parameters such as variation grinding size during the production period of the deposit of tailings (Mulenshi et al., 2019, 2021; Pan et al., 2014). Therefore, if certain minerals occur in a particular particle size, they may segregate and accumulate in specific zones of the deposit (Lottermoser, 2010). This trend was evidenced in section 4.4, where Al, HREE, P, Ca, Fe, Cu and Pb concentrations presented lateral stratifications. Elements such as Fe, Cu, and Pb could have been associated with coarse particles and tended to settle near discharge points. While Al, HREE, P and Ca could have been associated with finer and lighter particle sizes and were settling further away.

On the other hand, in order to delimit the possible alteration fronts along the depth profile of the deposit of tailings, the distribution patterns of pyrite, chalcopyrite and calcite were analyzed, as they represent the most reactive minerals. In addition, we analyzed the Co (representative of the trends of Cu, S and Fe) and LREE (representative of the trends of REEs) concentrations obtained by total digestion, the geostatistical distribution model, and the results of the different sequential extraction steps. An oxidation zone with an extension between 3-5 m in depth was determined, characterized by a lesser relative abundance of pyrite, chalcopyrite, and calcite with respect to the deeper levels. In this layer, the sulfide minerals present low degrees of alteration and the absence of Fe (III) oxyhydroxides rims or coatings. Below the oxidation zone, the sulfides remain unchanged, with constant relative abundance percentages, up to the depth

744 range between 17-18 m. This layer was defined as the primary zone. Subsequently, towards
745 the deeper layers (> 17 m) a significant increase in pyrite and S concentrations occur, which are
746 reflected in the one-way ANOVA and Welch test analysis performed in section 4.4, and in steps
747 5 and 6 of the SEP. In addition, elements associated with pyrite such as Co, Cu and Fe, and
748 elements associated with apatite such as P, are slightly enriched at the bottom of the deposit of
749 tailings, mainly in the depth range 30 – 40 m (Fig. 4 and Fig. S6). This last layer was present in
750 the deepest sectors, specifically in the central and eastern sectors of the deposit of tailings
751 (Fig.7). It was considered as a primary zone enriched in pyrite and apatite. The highest
752 proportion of these minerals in depth was attributed to the combination of three factors: 1) the
753 tailings dam geometry and the gravitational deposition of heavier mineral particles in the tailings
754 slurry that promote the relative enrichment of pyrite and apatite in the deep zone; 2) limited
755 oxygen diffusion at the bottom of the deposit of tailings. Therefore, the biotic oxidation reactions
756 are dominant, and they could be restricted by the low availability of Fe (III) in solution, due to
757 neutral pH conditions and low water flow, preserving pyrite; 3) there is little information about
758 the mine that gave rise to the mine wastes, so it is possible that the older tailings represent a
759 more pyrite-enriched portion of the ore deposit respect more recent materials, or could even
760 correspond to materials from a different mine nearby the flotation plant.
761
762 According to the conceptual model proposed in Fig. 7, it is observed that the concentrations
763 of the LREE (present in greater proportion than the HREE) represented in the section of the
764 central-eastern area of the deposit of tailings, do not present enrichment in the areas deeper of
765 the deposit. This trend corresponds to the observations made in the geostatistical model and it
766 is probably associated with the double association of REEs with aluminosilicates and apatite
767 minerals.
768

769 Regarding pH conditions within the tailings deposit, paste pH values remain relatively
770 constant (around 7.9) along the depth profile which indicates a relative homogeneous
771 distribution of calcite. The neutral pH values, low water content of the mine residue and high
772 evaporation in arid climates diminish the mobility of the elements liberated from the oxidation
773 zone and limit the oxidation reactions to fine-grained horizons (relatively poor in sulfide
774 minerals) due to their higher water retention capacity (Dold and Fontboté, 2002). In addition, the
775 low-sulfides characteristic of tailings from IOCG reservoirs together with the restriction of the
776 mobility of their oxidation products, explains the absence of secondary efflorescent salts on the
777 surface and the development of a secondary mineral enrichment zone. The above indicates that
778 the deposit of tailings is environmentally safe, due to the restricted mobility of potential polluting
779 elements.
780
781 On the other hand, some important aspects to highlight for future revalorization studies are: 1.
782 The economic recovery of the REEs from the reprocessing of the tailings is improbable,
783 because they are associated with both aluminosilicates and apatite minerals. Which makes it
784 difficult to concentrate these elements as by-products. 2. The high content of magnetite could
785 allow economic recovery of Fe by magnetic separation. This method is currently being applied
786 profitably by CAP's subsidiary Compañía Minera del Pacífico (CMP), located near of El Buitre
787 tailings deposit. CMP produces pellet feed with tailings from the copper concentrator plant of
788 Compañía Contractual Minera Candelaria, with average Fe grades of 11.4 % (Compañía Minera
789 del Pacífico, 2020). 3. The elimination of impurities from the Fe concentrate could favor the
790 concentration of Cu and its possible economic recovery. In addition, it would allow to
791 concentrate pyrite and recover the Co associated with its crystalline structure.
792
793 Taking into consideration all the above mentioned characteristics, a 3D conceptual model
794 was drawn using Leapfrog. To facilitate the model visualization, it was decided to highlight

several representative 2D sections (Fig. 7a) of the Co concentrations along the deposit of tailings. Additionally, two detailed representative section of the Co and LREE concentrations of the central-eastern area of the deposit of tailings are shown. These sections were contrasted with the geostatistical modeling.

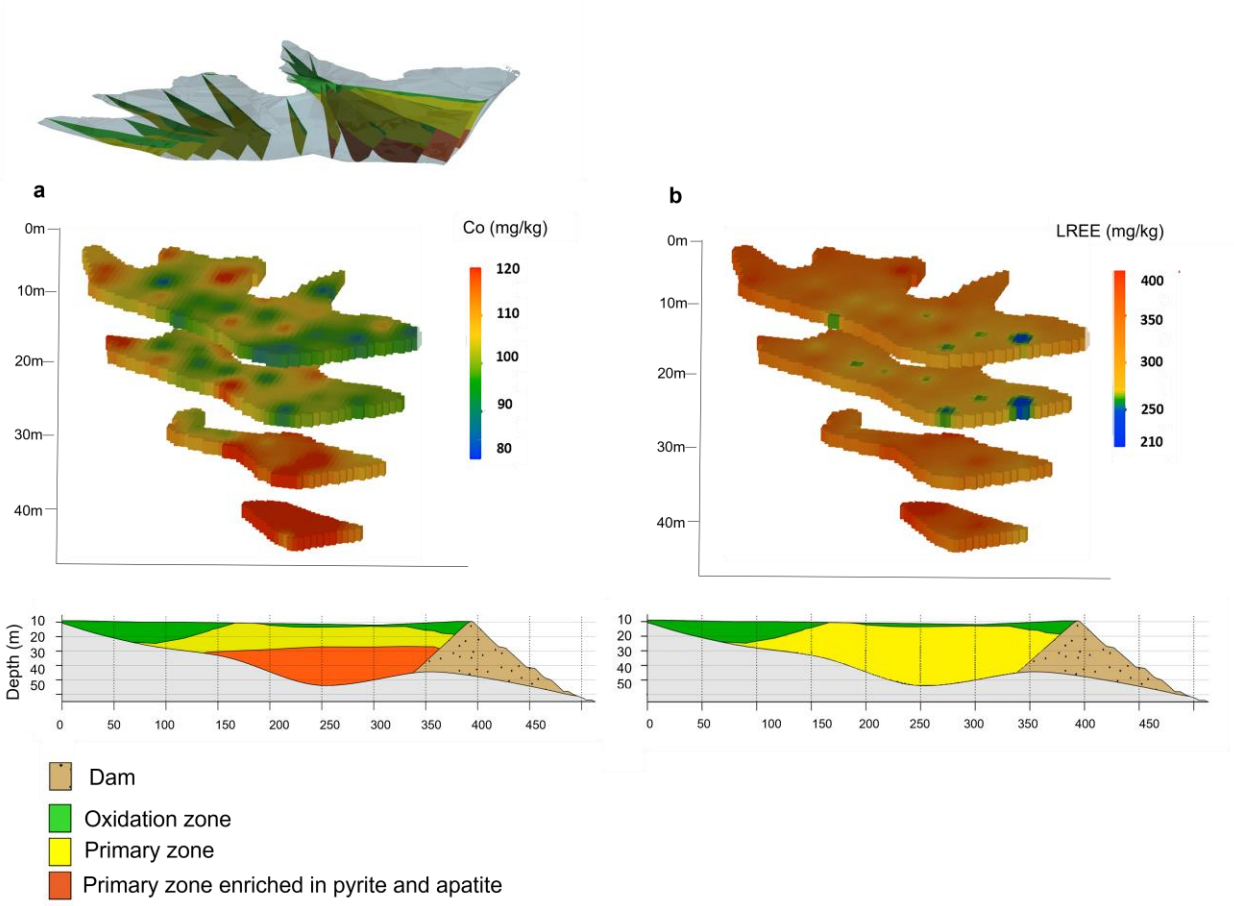

Fig. 7. a. Modeled Co concentration and cross-section of the distribution of the alteration fronts in the central-eastern area of the deposit of tailings. Additionally, the upper left figure shows different sections along the geometry of the deposit of tailings, indicating the absence of the layer enriched in sulfides and apatite, in the western sector of the deposit. b. Modeled LREE concentration and cross-section of the distribution of the alteration fronts in the central-eastern area of the deposit of tailings. This trend is representative of the distribution of REEs in the deposit of tailings.

6. Conclusions, implications, and future challenges

The following conclusions and implications can be extracted from the present study:

The low water flow in arid climates and the mobility restrictions of metals under neutral pore water pHs, inhibit the development of extensive oxidation fronts and mineral enrichment zones and prevent the appearance of efflorescent salts precipitated on the tailings surface. Therefore, the distribution of chemical elements is mainly controlled by the source deposit mineral composition, the mineral processing technology, gravitational deposition processes and the geometry of the deposit of tailings.

Due to the low mobility of potential polluting elements, the tailings dam presents a low risk of groundwater contamination, if the current environmental conditions remain.

The depositional history of this tailings deposit during its operation has shown the generation of layers with different geochemical and mineralogical characteristics (found at the bottom of this tailings deposit), that are unaffected by the limited supergenic weathering processes. These differences are most probably due to a different origin of the ore material processed in the mineral processing plant, whether it comes from a different section of the ore deposit with slightly different mineralogical characteristics (hydrothermal alteration zones, veins, etc.) or from a different mine located in the vicinity of the deposit of tailings.

Despite the presence of slight stratifications within the tailings deposit, from a reprocessing perspective, the geochemistry and mineralogy of the tailings is quite homogeneous, and it exhibits similar grades for potentially valuable elements (i.e., Fe, Cu, and Co) along the depth and horizontal profiles. Simplifying its exploration and exploitation for future revalorization

studies that could focus on the recovery of Fe by magnetic separation. This process could favor the concentration of Cu and Co in the purification stages of the magnetic concentrate. In contrast, the recovery of REEs as a by-product is improbable due to their double association, with apatite and aluminosilicate minerals.

The following future challenges are envisioned as a result of this study:

The relative homogeneity of the grades within the tailings deposit opens the possibility of restructuring the initial sampling mesh. Geostatistical studies are needed to evaluate the possibility of decreasing the number and density of boreholes while maintaining a robust and representative characterization of the deposit. This could drastically reduce the exploration cost of this marginally profitable secondary deposit.

Also, the present study has shown how limited the weathering and enrichment/depletion processes are in this type of neutral paste-pH tailings deposits in an arid climate. However, this slow mineral weathering cannot be neglected and robust hydrogeochemical models are needed to better understand the formation and evolution of these deposit of tailings stored (or to be stored) for decades. This information is essential to anticipate their long-term chemical stability and/or their possible generation of bigger and deeper oxidation zones within older deposits. To this end, another future challenge is to decipher the role played by microbial communities in the biogeochemical processes involved in the deposit of tailings weathering and evolution in time.

7. Acknowledgments

We gratefully acknowledge support from Codelco Tech and Pucobre S.A for their technical assistance during the sample collection process.

8. Author agreement

All authors read and approved the final manuscript.

9. Funding

This study was funded by CORFO and Codelco through the project 16PTECME-66524. It was also partially financed by the projects CONICYT/PIA Project AFB180004 and UNESCO-IUGS-IGCP-Project 682. Erika González-Díaz has received research support from the National Agency for Research and Development (ANID)/ Scholarship Program/ DOCTORADO BECAS CHILE/2019 -21192290. Manuel A Caraballo has received research supported from the Spanish Ministry of Science and Innovation through the Program Ramón y Cajal 2019, Grant RYC2019-026496-I.

10. References

Abraitis, P.K., Pattrick, R.A.D, Vaughan, D.J., 2004. Variations in the compositional, textural and electrical properties of natural pyrite: A review. International Journal of Mineral Processing 74(1–4):41–59. https://doi.org/10.1016/j.minpro.2003.09.002

Ahmadi, A., Khezri, M., Abdollahzadeh, A.A., Askari, M., 2015. Bioleaching of copper, nickel and cobalt from the low grade sulfidic tailings of Golgohar Iron Mine, Iran. Hydrometallurgy 154, 1e8. https://doi.org/10.1016/j.hydromet.2015.03.006.

879 Araya, N., Kraslawski, A., Cisternas, L.A., 2020. Towards mine tailings valorization: Recovery
880 of critical materials from Chilean mine tailings. Journal of Cleaner Production 263:121555.
881 https://doi.org/10.1016/j.jclepro.2020.121555
882
883 Araya, N., Ramírez, Y., Kraslawski, A., Cisternas, L., 2021. Feasibility of re-processing mine
884 tailings to obtain critical raw materials using real options analysis. Journal of Environmental
885 Management 284:112060. https://doi.org/10.1016/j.jenvman.2021.112060
886
887 Barton, M. D., 2014. Iron Oxide(-Cu-Au-REE-P-Ag-U-Co) Systems. In Treatise on
888 Geochemistry: Second Edition 13:515-541. Elsevier Ltd. https://doi.org/10.1016/B978-0-08-
889 095975-7.01123-2
890
891 Blowes, D., Jambor, J., Hanton-Fong, C., Lortie, L., Gould, W., 1998. Geochemical,
892 mineralogical and microbiological characterization of a sulphide-bearing carbonate-rich gold-
893 mine tailings impoundment, Joutel, Quebec. Journal of Applied Geochemistry 13(6):687–705.
894 https://doi.org/10.1016/S0883-2927(98)00009-2
895
896 Blowes, D.W., Ptacek, C.J., Jambor, J.L., Weisener, C.G., 2003. The Geochemistry of Acid
897 Mine Drainage. Treatise on Geochemistry, 9:149–204. https://doi.org/10.1016/B0-08-043751-
898 6/09137-4
899
900 Buch, A.C., Niemeyer, J.C., Marques, E.D., Silva-Filho, E.V., 2021. Ecological risk
901 assessment of trace metals in soils affected by mine tailings. Journal of Hazardous Materials
902 403:123852. https://doi.org/10.1016/j.jhazmat.2020.123852
903

Caraballo, M.A., Serna, A., Macías, F., Pérez-López, R., Ruiz-Cánovas, C., Richter, P., Becerra-Herrera, M., 2018. Uncertainty in the measurement of toxic metals mobility in mining/mineral wastes by standardized BCR®SEP. Journal of Hazardous Materials 360:587–593. https://doi.org/10.1016/j.jhazmat.2018.08.046

Ceniceros-Gómez, A.E., Macías-Macías, K.Y., de la Cruz-Moreno, J.E., Gutiérrez-Ruiz, M.E., Martínez-Jardines, L.G., 2018. Characterization of mining tailings in México for the possible recovery of strategic elements. Journal of South American Earth Sciences 88:72–79. https://doi.org/10.1016/j.jsames.2018.08.013

Cleaver, A.E, Jamieson, H.E., Rickwood, C.J., Huntsman, P., 2021. Tailings dust characterization and impacts on surface water chemistry at an abandoned Zn-Pb-Cu-Au-Ag deposit. Journal Applied Geochemistry 128:104927. https://doi.org/10.1016/j.apgeochem.2021.104927

Compañía Contractual Minera Candelaria, 2013. Expediente de Evaluación de Impacto Ambiental proyecto Candelaria 2030-Continuidad Operacional. Región de Atacama, Chile. https://seia.sea.gob.cl/documentos/documento.php?idDocumento=2128574336

Compañía Minera del Pacífico, 2020. Memoria anual 2020. 31(3):177. https://doi.org/10.5944/reop.vol.31.num.3.2020.29271

Daily metal prices, 2022. https://www.dailymetalprice.com/metalprices.php?c=fe&u=kg&d=1. Accessed 02-24-2022.

Deditius, A.P., Utsunomiya, S., Reich, M., Kesler, S.E., Ewing, R.C., Hough, R., Walshe, J., 2011. Trace metal nanoparticles in pyrite. Ore Geology Reviews 42(1):32–46. https://doi.org/10.1016/j.oregeorev.2011.03.003

Deutsch, C., Journel, A., 1997. GSLIB: Geostatistical Software Library and User's Guide. Oxford University Press, New York, pp. 369 (ISBN-13: 978-0195100150).

Dino, G.A., Mehta, N., Rossetti, P., Ajmone-Marsan, F., De Luca D.A., 2018. Sustainable approach towards extractive waste management: Two case studies from Italy. Resources Policy 59:33–43. https://doi.org/10.1016/j.resourpol.2018.07.009

Dold, B., Fontboté, L., 2001. Element cycling and secondary mineralogy in porphyry copper tailings as a function of climate, primary mineralogy, and mineral processing. Journal of Geochemical Exploration 74(1–3): 3–55. https://doi.org/10.1016/S0375-6742(01)00174-1

Dold, B., Fontboté, L., 2002. A mineralogical and geochemical study of element mobility in sulfide mine tailings of Fe oxide Cu - Au deposits from the Punta del Cobre belt, northern Chile. Chemical Geology 189(3–4):135–163. https://doi.org/10.1016/S0009-2541(02)00044-X

European Comission, 2017. Critical Raw Materials and the Circular Economy. Background report. In Report EUR 28832 EN. https://doi.org/10.2760/378123

Falagán, C., Grail, B.M., Johnson, D.B., 2017. New approaches for extracting and recovering metals from mine tailings. Minerals Engineering 106:71–78. https://doi.org/10.1016/j.mineng.2016.10.008

955 Franks, D.M., Stringer, M., Torres-Cruz, L.A., Baker, E., Valenta, R., Thygesen, K., Matthews,
956 A., Howchin, J., Barrie, S., 2021. Tailings facility disclosures reveal stability risks.
957 Scientific Reports 11(1):1–7. https://doi.org/10.1038/s41598-021-84897-0
958
959 Hällström, L.P.B., Alakangas, L., Martinsson, O., 2018. Geochemical characterization of W,
960 Cu and F skarn tailings at Yxsjöberg, Sweden. Journal of Geochemical Exploration 194:266–
961 279. https://doi.org/10.1016/j.gexplo.2018.09.001
962
963 Heikkinen, P.M., Räisänen, M.L., 2008. Mineralogical and geochemical alteration of Hitura
964 sulphide mine tailings with emphasis on nickel mobility and retention. Journal of Geochemical
965 Exploration 97(1):1–20. https://doi.org/10.1016/j.gexplo.2007.09.001
966
967 Henderson, R.D., 2018. Minera Valle Central Operations Rancagua, Region VI, Chile. 43–
968 101 Technical report. pp. 118. http://www.amerigoresources.com/_resources/
969 Technical_Report_March_2019.pdf (Accessed 2/20/2021).
970
971 Henne, A., Craw, D., Gagen, E.J., Southam, G., 2019. Bacterial influence on storage and
972 mobilisation of metals in iron-rich mine tailings from the Salobo mine, Brazil. Science of the
973 Total Environment 680:91–104. https://doi.org/10.1016/j.scitotenv.2019.04.448
974
975 Henne, A., Hamilton, J., Craw, D., Paterson, D., Southam, G., 2020. The influence of metal
976 mobility on resource potential in circumneutral pH iron-rich copper mine waste rocks. Journal of
977 Geochemical Exploration 219:106632. https://doi.org/10.1016/j.gexplo.2020.106632
978
979 Hites, R.A., 2019. Correcting for Censored Environmental Measurements. Environmental
980 Science and Technology 53(19):11059–11060. https://doi.org/10.1021/acs.est.9b05042

Kang, X., Gan, Y., Chen, R., Zhang, C., 2021. Sustainable eco-friendly bricks from slate tailings through geopolymerization: synthesis and characterization analysis. Construction and Building Materials 278:122337. https://doi.org/10.1016/j.conbuildmat.2021.122337

Kokkola, M., 1986. Jätealueen soijatutkimus. Outokumpu Oy Report 061/2124/02b/ MK/1986. pp. 83. http://tupa.gtk.fi/raportti/arkisto/061_2124_02b_mk_86.pdf

Kovács, E., Dubbin, W.E., Tamás, J., 2006. Influence of hydrology on heavy metal speciation and mobility in a Pb-Zn mine tailings. Environmental Pollution 141(2):310–320. https://doi.org/10.1016/j.envpol.2005.08.043

Krishna, R.S., Shaikh, F., Mishra, J., Lazorenko, G., Kasprzhitskii, A., 2021. Mine tailings-based geopolymers: Properties, applications and industrial prospects. Ceramics International 47(13): 17826-17843. https://doi.org/10.1016/j.ceramint.2021.03.180

Lam, E.J., Montofré, I.L., Álvarez, F.A., Gaete, N.F., Poblete, D.A., Rojas, R.J., 2020. Methodology to prioritize chilean tailings selection, according to their potential risks. International Journal of Environmental Research and Public Health 17(11):3948. https://doi.org/10.3390/ijerph17113948

Lam, E.J., Montofré, Í.L., Ramírez, Y., 2021. Mine tailings phytoremediation in arid and semiarid environments. In Phytorestoration of Abandoned Mining and Oil Drilling Sites 2021:115-116. https://doi.org/10.1016/b978-0-12-821200-4.00012-1

Liang, X., Wei, G., Xiong, J., Tan, F., He, H., Qu, C., Yin, H., Zhu, J., Zhu, R., Qin, Z., Zhang, J., 2017. Adsorption isotherm, mechanism, and geometry of Pb(II) on magnetites substituted

with transition metals. Chemical Geology 470:132–140. https://doi.org/10.1016/j.chemgeo.2017.09.003

LME, 2020. London metal exchange: LME cobalt and copper [WWW Document]. URL. https://www.lme.com/en/Metals/Accessed 02/24/2022.

Lindsay, M.B.J., Blowes, D.W., Condon, P.D., Ptacek, C.J., 2009a. Managing pore-water quality in mine tailings by inducing microbial sulfate reduction. Environmental Science and Technology 43(18):7086–7091. https://doi.org/10.1021/es901524z

Lindsay, M.B.J., Condon, P.D., Jambor, J.L., Lear, K.G., Blowes, D.W., Ptacek, C.J., 2009b. Mineralogical, geochemical, and microbial investigation of a sulfide-rich tailings deposit characterized by neutral drainage. Journal Applied Geochemistry 24(12):2212–2221. https://doi.org/10.1016/j.apgeochem.2009.09.012

Lottermoser, B.G., 2010. Mine Wastes (third edition): Characterization, treatment and environmental impacts, Mine Wastes (Third Edition): Characterization. Treatment and Environmental Impacts. https://doi.org/10.1007/978-3-642-12419-8.

Marescotti, P., Azzali, E., Servida, D., Carbone, C., Grieco, G., de Capitani, L., Lucchetti, G., 2010. Mineralogical and geochemical spatial analyses of a waste-rock dump at the Libiola Fe-Cu sulphide mine (Eastern Liguria, Italy). Environmental Earth Sciences 61(1):187–199. https://doi.org/10.1007/s12665-009-0335-7

Marschik, R., Fontboté, L., 2001. The Punta del Cobre formation, Punta del Cobre-Candelaria area, Northern Chile. Journal of South American Earth Sciences 14(4):401–433. https://doi.org/10.1016/S0895-9811(01)00036-0

Medina Tripodi, E.E., Gamboa Rueda, J.A., Aguirre Céspedes, C., Delgado Vega, J., Collao Gómez, C., 2019. Characterization and geostatistical modelling of contaminants and added value metals from an abandoned Cu–Au tailings dam in Taltal (Chile). Journal of South American Earth Sciences 93:183–202. https://doi.org/10.1016/j.jsames.2019.05.001

Mineralprices.com, 2022. Rare earth metals [WWW Document]. URL. http:// mineralprices.com/rare-earth-metals/. Accessed 02-24-2022.

Ministerio de obras públicas de Chile, 2020. Dirección General de Aguas, Chile. https://snia.mop.gob.cl/BNAConsultas/reportes

Ministerio Secretaría General de la Presidencia de Chile, 2002. Decreto 46. Norma de emisión de residuos líquidos a aguas subterráneas. http://bcn.cl/2eq80

Moncur, M.C., Ptacek, C.J., Blowes, D.W., Jambor, J.L., 2005. Release, transport and attenuation of metals from an old tailings impoundment. Journal Applied Geochemistry 20(3):639–659. https://doi.org/10.1016/j.apgeochem.2004.09.019

Moran-Palacios, H., Ortega-Fernandez, F., Lopez-Castaño, R., Alvarez-Cabal, J.V., 2019. The Potential of Iron Ore Tailings as Secondary Deposits of Rare Earths. Applied Sciences 9(14): 2913. https://doi.org/10.3390/app9142913

Mudd, G.M., Jowitt, S.M., 2018. Global Resource Assessments of Primary Metals: An Optimistic Reality Check. *Nat Resour Res* **27,** 229–240. https://doi.org/10.1007/s11053-017-9349-0

Mudd, G.M., Weng, Z., Jowitt, S.M., Turnbull, I.D., Graedel, T.E., 2013. Quantifying the recoverable resources of by-product metals: the case of cobalt. Ore Geol. Rev. 55, 87–98.

Mulenshi, J., Khavari, P., Chehreh Chelgani, S., Rosenkranz, J., 2019. Characterization and beneficiation options for tungsten recovery from Yxsj¨oberg historical ore tailings. Processes 7, 895. https://doi.org/10.3390/pr7120895.

Mulenshi, J., Gilbricht, S., Chehreh Chelgani, S., Rosenkranz, J., 2021. Systematic characterization of historical tailings for possible remediation and recovery of critical metals and minerals – The Yxsj¨oberg case. Journal of Geochemical Exploration 226: 106777. https://doi.org/10.1016/j.gexplo.2021.106777

Oyarzun, R., Rodríguez, M., Pincheira, M., Doblas, M., Helle, S., 1999. The Candelaria (Cu-Fe-Au) and Punta del Cobre (Cu-Fe) deposits (Copiapo, Chile): A case for extension-related granitoid emplacement and mineralization processes? Mineralium Deposita 34(8):799–801. https://doi.org/10.1007/s001260050241

Onyedika, G.O., Achusim-Udenko, A.C., Nwoko, C.I.A., Ogwuegbu, M.O.C., 2012. Chemistry, processes and problems of complex ores utilization: hydrometallurgical options. Int. J. Chem. Sci. 10, 112e130.

1082 Paktunc, D., Kingston, D., Pratt, A., McMullen, J., 2006. Distribution of gold in pyrite and in
1083 products of its transformation resulting from roasting of refractory gold ore. Canad Mineral 44(1):
1084 213–227. https://doi.org/10.2113/gscanmin.44.1.213
1085
1086 Pan, H., Zhou, G., Cheng, Z., Yang, R., He, L., Zeng, D., Sun, B., 2014. Advances in
1087 geochemical survey of mine tailings project in China. Journal of Geochemical Exploration
1088 139:193–200. https://doi.org/10.1016/j.gexplo.2013.07.012
1089
1090 Parbhakar-Fox, A., Glen, J., Raimondo, B., 2018. A Geometallurgical Approach to Tailings
1091 Management: An Example from the Savage River Fe-Ore Mine, Western Tasmania. Minerals 8,
1092 454; doi:10.3390/min8100454
1093
1094 Parviainen, A., 2009. Tailings mineralogy and geochemistry at the abandoned Haveri Au–Cu
1095 mine, SW Finland. Mine Water Environ. 28 (4), 291–304.
1096
1097 Parviainen, A., Soto, F., Caraballo, M.A., 2020. Revalorization of Haveri Au-Cu mine tailings
1098 (SW Finland) for potential reprocessing. Journal of Geochemical Exploration 218:106614.
1099 https://doi.org/10.1016/j.gexplo.2020.106614
1100
1101 Petrunic, B.M., Al, T.A., 2005. Mineral/water interactions in tailings from a tungsten mine,
1102 Mount Pleasant, New Brunswick. Geochimica et Cosmochimica Acta 69(10):2469–2483.
1103 https://doi.org/10.1016/j.gca.2004.10.031
1104

Sernageomin, 2020a. Catastro de Depósitos de Relaves En Chile. Servicio Nacional de Geología y Minería de Chile. https://www.sernageomin.cl/datos-publicos-deposito-de-relaves/. Accessed 17 May 2021

Sernageomin, 2020b. Datos de Geoquímica de Depósitos de Relaves En Chile. Servicio Nacional de Geología y Minería de Chile. https://www.sernageomin.cl/datos-publicos-deposito-de-relaves/. Accessed 20 June 2021

Sillitoe, R.H., 2003. Iron oxide-copper-gold deposits: An Andean view. Mineralium Deposita 38(7):787–812. https://doi.org/10.1007/s00126-003-0379-7

Sistema de información integral de Riego, 2020. Mapa de Evapotranspiración. Comisión nacional de riego, Chile. https://esiir.cnr.gob.cl/exp/ficha.php. Accessed 15 August 2021.

Smuda, J., Dold, B., Spangenberg, J.E., Friese, K., Kobek, M.R., Bustos, C.A., Pfeifer, H.R., 2014. Element cycling during the transition from alkaline to acidic environment in an active porphyry copper tailings impoundment, Chuquicamata, Chile. Journal of Geochemical Exploration 140:23–40. https://doi.org/10.1016/j.gexplo.2014.01.013

Soto, F., Garrido, M., Diaz, G., Silva, C., 2017. Rapid Multivariate Resource Assessment. Geomin-mineplanning. 5th International Seminar on Geology for the Mining Industry, Santiago

Su, W., 2009. Economic and Policy Analysis of China's Rare Earth Industry. China Financ. Econ. Publ House, Beijing.

Tremblay G.A., Hogan, C.M., 2000. MEND Manual Volume 5–Treatment. 5:187

USGS, 2000. Open-File report OFR01-041. Coastal and Marine Geology Program website. https://pubs.usgs.gov/of/2001/of01-041/htmldocs/methods.htm. Accessed 16 June 2021

Wang, L., Li, Y., Wang, H., Cui, X., Wang, X., Lu, A., Wang, X., Wang, C., Gan, D., 2017. Weathering behavior and metal mobility of tailings under an extremely arid climate at Jinchuan Cu-Ni sulfide deposit, Western China. Journal of Geochemical Exploration 173:1–12. https://doi.org/10.1016/j.gexplo.2016.11.009

Yang, M., Liang, X., Ma, L., Huang, J., He, H., Zhu, J., 2019. Adsorption of REEs on kaolinite and halloysite: A link to the REEs distribution on clays in the weathering crust of granite. Chemical Geology 525: 210–217. https://doi.org/10.1016/j.chemgeo.2019.07.024

Zhang, N., Tang, B., Liu, X., 2021. Cementitious activity of iron ore tailings and its utilization in cementitious materials, bricks and concrete. Construction and Building Materials 288:123022. https://doi.org/10.1016/j.conbuildmat.2021.123022

	Min.	Max.	Mean	Median	SD	Percentiles			
Major						25.0	50.0	75.0	95.0
Fe	9	26	16	15	2	14	15	17	20
Al	1	10	5	5	2	4	5	6	8
Ca	2	6	3	3	1	2	3	3	4
Mg	1	5	2	2	1	2	2	3	3
Si* (XRF)	0.2	3	2	2	0.4	1	2	2	2
K	0.7	5	2	2	0.4	2	2	3	3
S	0.2	3	2	2	0.4	1	2	2	2
Na	0.3	2	0.9	0.9	0.3	0.7	0.9	1	2
Ti	0.1	1	0.3	0.3	0.1	0.2	0.3	0.3	0.3
P	0.1	0.2	0.1	0.1	0.0	0.1	0.1	0.1	0.2
Minor									
Cu	227	4290	795	647	514	433	647	990	1790
LREE	67	800	315	306	110	234	306	373	520
V	62	579	108	105	29	91	106	121	150
Co	25	303	103	100	32	83	100	120	158
Trace									
Ni	28	178	79	76	22	63	76	93	121
Zn	35	196	63	60	18	50	60	71	93
As	1	107	38	37	12	30	37	43	59
Li	14	79	30	26	10	22	26	33	52
Ga	14	41	24	25	5	19	25	28	32
HREE	10	44	22	22	5	18	22	25	30
Pb	2	38	12	11	6	8	11	16	24
W	0	101	7	6	6	4	6	8	12
Th	1	9	3	3	1	3	3	4	5
Sn	1	18	3	2	2	2	2	3	5
Cs	1	7	2	2	1	1	2	2	3
U	1	3	2	2	0.3	2	2	2	2
Ag	0.1	4	1	1	1	1	1	1	2
Mo	0.1	4	1	1	1	1	1	1	2
Be	1	3	1	1	0.3	1	1	1	2
Ge	0.1	2	1	1	0.4	0.3	1	1	1
Bi	0.1	4	1	1	0.3	0.4	1	1	1

1149

1150 Table 1. Univariate statistics for selected elements of the tailings with Min., Max., Mean, Median,
1151 standard deviation (SD) and percentiles (25, 50, 75 and 95). Major elements in % wt and minor
1152 and trace elements in mg/kg. The concentrations correspond to the total digestion analysis (N=
1153 755 samples). The concentration of Cd, Ba, Cr, Nb, Sb and Se were below the detection limit.

Elements	Cut-off	Mean grade	Percentage (%)	Reserves (Mt)	Metal prices[a] (US$/ton)	Economic potential (MUS$)
REEs	200 mg/kg	337 mg/kg	100	0.0022	4651315	10232.9
Co	190 mg/kg	103 mg/kg	0	0	72780	-
Cu	0.10 wt %	0.07 wt %	2.1	0.00009	9929	0.9
Fe	11.4 wt %	15.50 wt %	100	1.023	141.1	144345.3

1154 [a] Sources: (LME, 2022), Daily metal prices (2022) and Mineralprices.com (2022)

1155 Table 2. Rough estimation of potential resources of El Buitre tailings deposit

Steps	1	2	3	4	5	6	7
Aluminum			Mean ±SD				
Depth (m)							Silicates
1	<DL	18 ± 5	54 ± 5	43 ±2	12 ± 1	246 ± 12	1633 ± 10 a
3	<DL	26 ± 5	64 ± 3	44 ±3	14 ± 0	233 ± 10	1620 ± 3 a
9	<DL	18± 5	55 ± 11	45 ± 10	13 ± 3	259 ± 82	1415 ± 162 a
15	<DL	17 ± 1	68 ± 2	52 ± 1	15 ± 0	315 ± 62	1612 ± 37 a
21	<DL	18 ± 4	68 ± 5	45 ± 7	15 ± 1	310 ± 38	1456 ± 38 a
35	<DL	19 ± 0	82 ± 11	57 ± 2	20 ± 5	408 ± 48	1425 ± 100 a
Calcium	Gypsum	Carbonates					
1	137 ± 31 a	297 ± 84 a	<DL	<DL	52 ± 5	21 ± 0	53 ± 44
3	108 ± 32 a	411 ± 114 ab	<DL	<DL	69 ± 11	23 ± 5	22 ± 4
9	107 ± 16 a	564 ± 26 b	<DL	<DL	91 ± 15	34 ± 5	<DL
15	99 ± 1 a	616 ± 43 b	<DL	<DL	109 ± 6	31 ± 1	<DL
21	138 ± 69 a	625 ± 61 b	<DL	<DL	105 ± 3	33 ± 1	19 ± 6
35	128 ± 25 a	806 ± 83 c	<DL	<DL	140 ± 24	38 ± 1	<DL
Sulphur	Gypsum				Secondary sulfide	Primary sulfide	
1	134 ± 33 a	<DL	<DL	<DL	274 ± 7 a	68 ± 12 a	<DL
3	120 ± 7 a	<DL	<DL	<DL	324 ± 33 ab	146 ± 5 b	40 ± 6
9	83 ± 5 a	<DL	<DL	<DL	404 ± 27 ab	137 ± 69 b	33 ± 1
15	96 ± 1 a	<DL	<DL	<DL	418 ± 14 ab	78 ± 7 a	<DL
21	140 ± 76 a	<DL	<DL	<DL	432 ± 16 ab	159 ± 18 b	16 ± 9
35	128 ± 27 a	<DL	<DL	<DL	497 ± 13 b	164 ± 62 b	12 ± 1
Copper					Secondary sulfide	Primary sulfide	
1	<DL	6 ± 1	5 ± 1	0.6 ± 0	5 ± 0.3 a	1 ± 0.1 a	0.3 ± 0.1
3	<DL	4 ± 0	2 ± 0	0.3 ± 0	10 ± 2 b	2 ± 1 a	0.3 ± 0
9	<DL	2 ± 0	2 ± 0	0.3 ± 0	4 ± 0.1 a	1 ± 0.1 a	0.3 ± 0.1
15	<DL	2 ± 0	1 ± 0	0.3 ± 0	3 ± 0.1 a	0.7 ± 0.1 a	0.2 ± 0
21	<DL	2 ± 0	2 ± 1	0.3 ± 0	5 ± 1 a	1 ± 0.1 a	0.1 ± 0
35	<DL	5 ± 1	3 ± 1	0.5 ± 0	13 ± 0.1 b	2 ± 0 b	0.3 ± 0.1
Iron			Fe (III) Oxyhydroxides	Fe (III) Oxides			Silicates
1	<DL	31 ± 9	289± 24 a	178 ± 24 a	74 ± 1	538 ± 10	1637 ± 3
3	<DL	44 ± 6	258± 2 a	192 ± 9 a	85 ± 3	583 ± 13	1716 ± 188
9	<DL	38 ± 8	291 ±10 a	195 ± 19 a	116 ± 17	626 ± 60	1902 ± 139
15	<DL	43 ± 1	270±18 a	193 ± 18 a	136 ± 14	664 ± 84	1492 ± 216
21	<DL	38 ± 9	320±79 a	201 ± 11 a	127 ± 15	706 ± 103	1570 ± 234
35	<DL	41 ± 1	302±17 a	206 ± 18 a	151 ± 18	825 ± 38	1155 ± 0

Table 3. Results of the sequential extraction corresponding to the average of boreholes Ad2, B-04 and B-13. The values are expressed in mmol/kg. Elements below the detection limit are indicated as <DL. Step 1: Water soluble fraction. Step 2: Exchangeable fraction, Step 3: Fe (III) oxyhydroxides, Step 4: Fe (III) oxides, Step 5: Organics and secondary Cu-sulfides, Step 6: Primary sulfides and Step 7: Residual fraction. Different letters indicate that there is a significant difference between the concentration of the elements at a certain depth. On the contrary, the same letters indicate that there are no significant differences.